Progress In Electromagnetics Research B, Vol. 53, 373–397, 2013

CIRCUIT APPROACH TO THE ANALYSIS OF MICROWAVE DISCONTINUITIES

Leonardo Zappelli*

Dipartimento di Ingegneria dell'Informazione, Università Politecnica delle Marche, Via Brecce Bianche, Ancona 60131, Italy

Abstract—An equivalent circuit based on propagating and evanescent accessible modes is discussed and the numerical values of its elements (susceptances and electrical length) are obtained starting from the knowledge of the generalized scattering matrix S of microwave discontinuities. A database of the circuit elements is then defined in the frequency and geometric ranges of the analyzed discontinuities and is used to evaluate the generalized scattering matrix for values not contained in the database, with very simple formulas for any number of circuit ports. The obtained S matrices can be used to analyze very complex structures such as iris-based filters and manifold filters.

1. INTRODUCTION

Manifold multiplexers are structures which permit several channels or signals to be combined into a single waveguide. They are widely used in satellite equipment to satisfy filtering and channel performance requirements [1–4]. Unfortunately, the satellite equipment should be as compact as possible in order to reduce the weight of the overall transmission system. These constraints call for very close interacting discontinuities in the filters or multiplexers (irises, posts, screws, ...) in order to minimize the dimensions of the overall structures. This means that evanescent accessible modes interacting between very close discontinuities must be taken into account in the development of the filters and the final optimization of the multiplexer. The final optimization of the dimension of separations and widths of the interacting discontinuities should be very effective if a good equivalent circuit of each discontinuity is considered. The equivalent circuit should contain the effects of propagating and evanescent accessible

Received 10 June 2013, Accepted 10 August 2013, Scheduled 15 August 2013

* Corresponding author: Leonardo Zappelli (l.zappelli@univpm.it).

modes at the same time so as to correctly simulate the interactions with the discontinuities.

In the past, a great number of equivalent circuits have been analyzed and the results can be found in two excellent books [5, 6]. While these circuits were very useful between the 1950s and the 1970s, they are limited to propagating modes alone and therefore they are currently not often used because they are not able to simulate the effects of very close interacting discontinuities exciting evanescent accessible modes.

Recently, an accurate equivalent circuit representing the effect of a discontinuity on the propagating and evanescent accessible modes has been proposed [7]. In this equivalent circuit, which can easily be drawn for any numbers of ports (modes), unlike other recently discussed equivalent circuits [8], an evanescent mode is represented by an evanescent line of electrical length θ connected with a series reactance equal to the conjugate of the modal (reactive) impedance and a transformer that links the modal port to the "core" of the circuit, based on an n-sides polygon with susceptances placed on every side and diagonal. The propagating modes have a similar representation apart from the presence of the series reactance which disappears for these modes. An example based on a five-port model with one input propagating mode, one output propagating mode and three output evanescent accessible modes is shown in Fig. 1.

Even if the number of excited evanescent accessible modes increases, the manipulation of the proposed equivalent circuit is still easy and feasible. As an example, let us suppose that two closed discontinuities represented by two five-port equivalent circuits, such as that shown in Fig. 1, are interacting. The total equivalent circuit is obtained by cascading the two equivalent circuits, connecting the output ports of the first circuit with the input ports of the second. Although the overall circuit could seem very complicated, it can easily be solved thereby, obtaining the scattering matrix of the two discontinuities cascade. In fact, it can be solved by using classical solutions for electric networks, as Kirchoff's laws KVL and KCL, to evaluate the overall Z_{tot} matrix and subsequently the generalized scattering matrix S_{tot} matrix, or by "cascading" the S matrices of the two discontinuities, if they are known. In this paper, the derivation of the S matrix for the n-port equivalent circuit will be discussed and will be evaluated with simple formulas.

The aim of the present paper is to propose a circuit approach based on the equivalent circuit with n ports to describe microwave networks and to provide the numerical values of the electrical parameters of the circuits for researchers working on this topic, just as Marcuvitzs

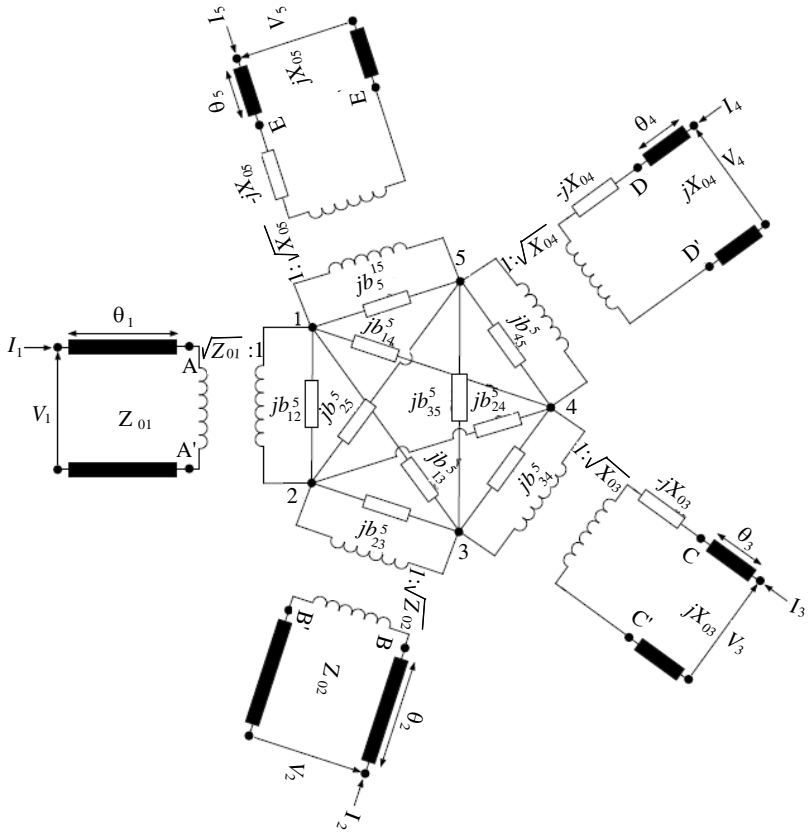

Figure 1. The equivalent five-port circuit for a discontinuity with one input, one output propagating mode (ports 1, 2) and three output evanescent modes (ports 3, 4, 5) [7].

Handbook [5] did in the 50s. Obviously, this is a long-term intent, as the number of discontinuities analyzed in the Handbook is very large. Moreover, the Author is willing to provide these data with the help of Internet, sharing them with an open-source agreement on a web platform (the data can be downloaded as described in the following sections). To that end, first the S-parameters must be known at some frequency points and this can be done with commercial or self-developed software. These values are then used to obtain the n-port circuit parameters (susceptances and electrical lengths) exactly at these points and they are shared on Internet. If a researcher needs the S-parameters at the same frequency, he can use the database previously downloaded (or stored) to re-build the S-parameters at

the frequency points of interest. The reconstruction of the n-port (with n being even very large) is made by Eqs. (1)–(11). If the researcher needs the S-parameter points at frequency points different from those previously obtained, he can use the linear interpolation on the downloaded database as described in the following sections, with little effort in terms of code programming. Hence, some equivalent circuits referring to H-plane bends and thick irises, either centered or not, will be obtained and they will be used to build the database that will be used to evaluate the characteristics of the filters/multiplexers discussed in the literature, showing good agreement.

It is important to emphasize that, to the Author's knowledge, there is no description in literature on how to easily draw a circuit with n ports, representing a discontinuity exciting n modes, with $n*(n+1)/2$ impedances (if the S matrix is symmetric). Examples of three port circuits, characterized by 6 impedances, can be found, as in Marcuvitzs Handbook [5], but they appear to be complex and not so simple as the proposed circuit. Examples of drawing four or five port circuits (with 10 or 15 impedances) are just as difficult to find. If a similar circuit was drawn, the derivation of its S matrix could be made, but the extension to a circuit with any number of ports would be very hard. Hence, the Author thinks that the proposed circuit permits the problem of drawing an n port circuit to be easily solved and its S matrix can be obtained by means of Eqs. (1)–(11), with very little effort in terms of software implementation.

2. THEORY

Let us consider the 5-port equivalent circuit shown in Fig. 1 [7]. It refers to the case of a discontinuity characterized by one input and one output propagating mode (ports 1 and 2) and three output evanescent accessible modes (ports 3, 4 and 5). Ports 1 and 2 have real modal impedances Z_{01} and Z_{02} and ports 3, 4 and 5 purely imaginary ones jX_{03}, jX_{04} and jX_{05}. The input/output ports are connected with transmission lines of electrical lengths θ_k, $k = 1, 2, \ldots, 5$ and with five transformers to the "core" of the circuit, based on a pentagon with susceptances b_{ij}^5 on every side and diagonal. The presence of series reactances $-jX_{0k}$, $k = 3, 4, 5$ connected to the lines referring to evanescent modes should be noted. These reactances are the key of the evanescent ports. In fact, if port 5 is connected to a very long line (or it is matched), the input impedance seen at terminal E-E' is equal to jX_{05} which resonates with the series reactance $-jX_{05}$, yielding a short circuit seen at the terminal 1–5. The short circuit simplifies the overall circuit, because node 5 disappears, being coincident with node

1. Moreover, susceptances b_{25}^5, b_{35}^5, b_{45}^5 are connected in parallel to b_{12}^5, b_{13}^5, b_{14}^5, respectively and the 5-port circuit reduces to the 4-port circuit shown in Fig. 3(a) of [7] with $b_{12}^4 = b_{12}^5 + b_{25}^5$, $b_{23}^4 = b_{23}^5$, $b_{34}^4 = b_{34}^5$, $b_{14}^4 = b_{45}^5 + b_{14}^5$, $b_{13}^4 = b_{13}^5 + b_{35}^5$, $b_{24}^4 = b_{24}^5$.

This reduction process can be applied again if port 4 is matched, or connected to a very long line. In this case, the circuit reduces to the 3-port one, shown in Fig. 3(b) of [7], with $b_{13}^3 = b_{13}^4 + b_{34}^4$, $b_{12}^3 = b_{12}^4 + b_{24}^4$, $b_{23}^3 = b_{23}^4$. In other words, the equivalent circuit proposed in [7] seems to be a "natural" equivalent circuit, in the sense stated by Marcuvitz [5]: a great number of circuits can be proposed and they are all correct, but only some of them seem to be a "natural" representation of the physics of the problem. In this case, the proposed circuit seems the most "natural" both to represent the presence of an evanescent accessible mode (and its disappearance, when it is matched or connected to a very long line), and to satisfy the properties of the S matrix in the presence of evanescent accessible modes [7].

If the number of accessible modes increases, the circuit is easily drawn and it is based on an n-polygon with susceptances on every side and diagonal. Each side is connected with a transformer and a line of electrical length θ_k to the port. If the port refers to an evanescent accessible mode, a serie reactance $-jX_{0k}$ is added between the transformer and the line, with jX_{0k} being the modal imaginary impedance of the k-th mode (port).

The proposed n-port circuit should be useful if its scattering matrix is easy to evaluate. In fact, the S matrix could be cascaded with other S matrices representing other discontinuities interacting with the n-port circuit. However the proposed circuit is unusable if its S matrix is very complex and difficult to evaluate. Fortunately, due to the circuit modularity, we can write its S matrix in a very simple

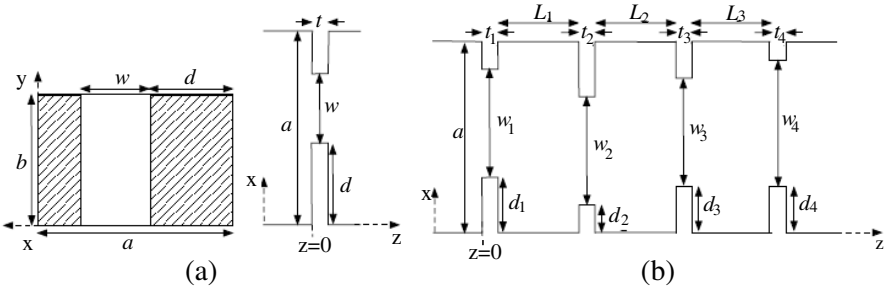

Figure 2. The cascade of four non-centered irises in a rectangular waveguide.

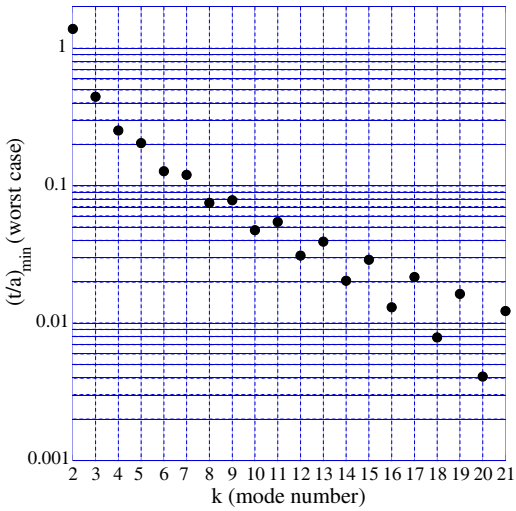

Figure 3. Minimum value of $\frac{t}{a}$ to neglect the k-th output evanescent mode of the regular-to-reduced-width waveguide transition, placed at $z = 0$ in Fig. 2(a), with $(\frac{d}{a}, \frac{w}{a}, \frac{f}{f_{c,1}})$ being fixed at the "worst" case.

form, starting from the knowledge of the generalized scattering matrix of the 4-port circuit shown in Fig. 3(a) of [7], with simple mathematical manipulations:

$$S_{11} = \frac{-b_p}{b_p - 2j}\, e^{-2j\theta_1} \tag{1}$$

$$S_{12} = \frac{-2j}{b_p - 2j}\, e^{-j(\theta_1+\theta_2)} \tag{2}$$

$$S_{22} = \frac{-b_p}{b_p - 2j}\, e^{-2j\theta_2} \tag{3}$$

$$S_{1k} = \frac{2e^{j\pi/4}}{b_p - 2j} \left(\sum_{m=3}^{k} b_{2m}^n - j \right) e^{-j\theta_1-\theta_k} \tag{4}$$

$$S_{1i} = \frac{2e^{j\pi/4}}{b_p - 2j} \left(-j + \sum_{m=3}^{k} b_{2m}^n + \sum_{m=k+1}^{i} b_{2m}^n \right) e^{-j\theta_1-\theta_i} \tag{5}$$

$$S_{2k} = -\frac{2e^{j\pi/4}}{b_p - 2j} \left(-j + b_{12}^n + \sum_{m=i+1}^{n} b_{2m}^n + \sum_{m=k+1}^{i} b_{2m}^n \right) e^{-j\theta_2-\theta_k} \tag{6}$$

$$S_{2i} = -\frac{2e^{j\pi/4}}{b_p - 2j}\left(-j + b_{12}^n + \sum_{m=i+1}^{n} b_{2m}^n\right) e^{-j\theta_2 - \theta_4} \tag{7}$$

$$S_{kk} = \left\{1 + 2\left[\sum_{l=k+1}^{i}\left(b_{kl}^n + \sum_{m=3}^{k-1} b_{ml}^n\right) + \sum_{m=3}^{k}\left(b_{1m}^n + \sum_{l=i+1}^{n} b_{ml}^n\right)\right] - 2\frac{1 + jb_p - \left[b_{12}^n + \sum_{m=i+1}^{n} b_{2m}^n + \sum_{m=k+1}^{i} b_{2m}^n\right]\sum_{m=3}^{k} b_{2m}^n}{b_p - 2j}\right\} e^{-2\theta_k} \tag{8}$$

$$S_{ki} = \left[2\sum_{m=3}^{k}\left(b_{1m}^n + \sum_{l=i+1}^{n} b_{ml}^n\right) + \frac{2\left(-j + b_{12}^n + \sum_{m=i+1}^{n} b_{2m}^n\right)\left(-j + \sum_{m=3}^{k} b_{2m}^n\right)}{b_p - 2j}\right] e^{-\theta_k - \theta_i} \tag{9}$$

$$S_{ii} = \left\{1 + 2\sum_{l=i+1}^{n}\left(b_{il}^n + \sum_{m=k+1}^{i-1} b_{ml}^n\right) + 2\sum_{m=3}^{k}\left(b_{1m}^n + \sum_{l=i+1}^{n} b_{ml}^n\right) + 2\frac{\sum_{m=3}^{k} b_{2m}^n + \sum_{m=k+1}^{i} b_{2m}^n}{b_p - 2j}\left(b_{12}^n + \sum_{m=i+1}^{n} b_{2m}^n\right) + 2\sum_{m=k+1}^{i} b_{1m} - 2\frac{1 + jb_p}{b_p - 2j}\right\} e^{-2\theta_i} \tag{10}$$

$$b_p = b_{12}^n + \sum_{m=3}^{n} b_{2m}^n \qquad k = 3, \ldots, n \quad i = k+1, \ldots, n \tag{11}$$

If the output section of the discontinuity is characterized by evanescent modes only, similar equations can be obtained. Details of these are available in the Appendix A. Once the S matrix for the n-port equivalent circuit has been obtained, it can be used together with its equivalent circuit to analyze a discontinuity with any number of evanescent modes that can interact with adjacent discontinuities.

3. NUMERICAL RESULTS

The purpose of this section is to evaluate the equivalent circuits which take into account the presence of a number of evanescent accessible modes and which can replace the corresponding circuits discussed in [5, 6], relative to propagating modes alone, for a number of discontinuities involved in the development of multiplexers/filters, such as irises (either centered or not), and bends. Obviously, these circuits are obtained using technical solutions and software that were not available when [5, 6] were written. Hence, our goal is to construct a number of databases containing the values of the electrical parameters (susceptances and electrical lengths) of the equivalent circuits for some values of the frequency and geometrical parameters of the discontinuities under investigation, which should replace the graphs contained in [5, 6]. Hence, with simple numerical interpolation on the database values, the electrical parameters of the n-port equivalent circuit can be obtained, in the same way in which, for example, the pure shunt of an H-plane bend can be obtained from the quasi-analytical formulas or from the graphical interpolation of the plots reported on pages 318–322 of [5]. The advantage of the proposed approach is the possibility to obtain the equivalent circuits based on propagating and evanescent accessible modes (not contained in [5]), which can be used to cascade with those of adjacent strong interacting discontinuities.

Once the electrical parameters for the real case have been interpolated from the corresponding databases, the n-ports S matrix can be obtained as discussed in the previous section and can be "cascaded" with the S matrices of the interacting adjacent discontinuities.

Hence, the first step is to analyze some discontinuities with a commercial or self-developed numerical software to obtain their numerical S matrices for some values of frequencies and geometrical parameters and to "fill" the susceptances and the electrical lengths of the n-port equivalent circuit with the corresponding values obtained using the approach described in [7]. We can then build the databases in the frequency and geometrical domains which permit some interpolating functions to be constructed which are useful for speeding up the analysis of the discontinuities in the frequency and geometrical points not contained in the built databases.

For example, referring to Fig. 2(a), the case of non-centered iris in a rectangular waveguide has been analyzed, by decomposing the iris in the cascade of

- a regular-to-reduced-width waveguide transition placed at $z = 0$ in Fig. 2(a)

- a reduced waveguide of length t and width w ($0 \leq z \leq t$)
- a reduced-to-regular-width waveguide transition placed at $z = t$ in Fig. 2(a)

and the S matrix of the first discontinuity at $z = 0$ (regular-to-reduced-width waveguide, named $S_{a \to w}$) has been evaluated with a self-developed electromagnetic code, based on the Multimode Equivalent Network (MEN) method [9–11], by varying the geometrical parameters w and d, in steps of $0.02a$, with a being the width of the rectangular waveguide, corresponding to 50 points in the w and d ranges. 21 accessible modes and 400 localized modes with 200 basis functions have been used in the simulations. The step in the frequency range $1.25 < \frac{f}{f_{c,1}} < 1.9$, where $f_{c,1}$ is the frequency cutoff of the fundamental mode of the regular waveguide of width a, has been set to $0.0065 f_{c,1}$, corresponding to 100 points. Finally, one propagating mode with 20 evanescent accessible modes has been used at the input side ($z = 0^-$) and one propagating mode with 20 evanescent modes at the output side ($z = 0^+$). The numerical values of the $S_{a \to w}$ matrix obtained at these points (20 for $\frac{w}{a}$, 20 for $\frac{d}{a}$ and 100 for $\frac{f}{f_{c,1}}$) have been used to evaluate the electrical lengths θ_k and the susceptances b_{ij}^n relative to an n-port equivalent circuit, with $n = 42$ ports. It should be noted that if the width w of the reduced waveguide is less than $0.52a$, its fundamental mode is below cutoff, and the output ports are all evanescent. The electrical lengths θ_k, $k = 1, \ldots, 42$ and the susceptances b_{ij}^n have been evaluated with the technique discussed in [7] and a database has been built for each θ_k and b_{ij}^n in the discretized 3-D variables space ($\frac{d_p}{a}$, $\frac{w_q}{a}$, $\frac{f_m}{f_{c,1}}$) with $p = 1, \ldots, 20$, $q = 1, \ldots, 20$ and $m = 1, \ldots, 100$.

A 3-D linear interpolation has then been defined on the database, in order to evaluate the electrical parameters of the equivalent circuit for values ($\frac{\bar{d}}{a}$, $\frac{\bar{w}}{a}$, $\frac{\bar{f}}{f_{c,1}}$) not contained in the database. For example, the value of the electrical length θ_1 at point ($\frac{\bar{d}}{a}$, $\frac{\bar{w}}{a}$, $\frac{\bar{f}}{f_{c,1}}$), with $\frac{d_p}{a} \leq \frac{\bar{d}}{a} \leq \frac{d_{p+1}}{a}$, $\frac{w_q}{a} \leq \frac{\bar{w}}{a} \leq \frac{w_{p+1}}{a}$, $\frac{f_m}{f_{c,1}} \leq \frac{\bar{f}}{f_{c,1}} \leq \frac{f_{m+1}}{f_{c,1}}$, can be obtained by the following interpolation:

$$\theta_1\left(\frac{\bar{d}}{a}, \frac{\bar{w}}{a}, \frac{\bar{f}}{f_{c,1}}\right) = D_{p,q,m} + \frac{\dfrac{\bar{d}}{a} - \dfrac{d_p}{a}}{\dfrac{d_{p+1}}{a} - \dfrac{d_p}{a}} \left(D_{p+1,q,m} - D_{p,q,m}\right) \quad (12)$$

$$D_{p,q,m} = W_{p,q,m} + \frac{\dfrac{\bar{w}}{a} - \dfrac{w_q}{a}}{\dfrac{w_{p+1}}{a} - \dfrac{w_q}{a}} \left[W_{p,q+1,m} - W_{p,q,m} \right] \tag{13}$$

$$W_{p,q,m} = \theta_1 \left(\frac{d_p}{a}, \frac{w_q}{a}, \frac{f_m}{f_{c,1}} \right) + \frac{\dfrac{\bar{f}}{f_{c,1}} - \dfrac{f_m}{f_{c,1}}}{\dfrac{f_{m+1}}{f_{c,1}} - \dfrac{f_m}{f_{c,1}}} \left[\theta_1 \left(\frac{d_p}{a}, \frac{w_q}{a}, \frac{f_{m+1}}{f_{c,1}} \right) - \theta_1 \left(\frac{d_p}{a}, \frac{w_q}{a}, \frac{f_m}{f_{c,1}} \right) \right] \tag{14}$$

Similar expressions can be obtained for the other electrical lengths θ_k and susceptances b_{ij}^n.

The 3-D linear interpolation (12)–(14) can been used to evaluate the equivalent circuit parameters and, subsequently, the S matrix (1)–(11) for points ($\frac{\bar{d}}{a}$, $\frac{\bar{w}}{a}$, $\frac{\bar{f}}{f_{c,1}}$) not contained in the built database.

The obtained $S_{a\to w}$ matrix has been "cascaded" with the S matrix of the straight reduced-width w of length t, placed at $0^+ \le z \le t^-$, (equivalent to a phase shift [12]) and then with the $S_{w\to a}$ matrix, placed at $z = t$, representing the reduced-to-regular-width waveguide transition, obtained by the inversion of the input and output ports of $S_{a\to w}$: the resulting S matrix represents that of the non-centered iris with thickness t.

A critical point in the discussion regarding this approach could be the question why the interpolating functions (12)–(14) are not directly applied to the elements of $S_{a\to w}$, without "transforming" the $S_{a\to w}$ matrix in the b_{ij}^n and θ_k of the equivalent circuit. In other words: why not build a database directly on the elements S_{ij} of $S_{a\to w}$, then apply the approximating functions (12)–(14) to the elements S_{ij} of $S_{a\to w}$ and finally reconstruct the $S_{a\to w}$ matrix in points of the 3-D space ($\frac{\bar{d}}{a}$, $\frac{\bar{w}}{a}$, $\frac{\bar{f}}{f_{c,1}}$) not contained in the built database? This approach would avoid the transformation to the equivalent circuit, obtaining the same goal.

The answer to this question is that, first of all, the database built on b_{ij}^n and θ_k is made only of $n(n+1)/2$ real numbers for any ($\frac{d_p}{a}$, $\frac{w_q}{a}$, $\frac{f_m}{f_{c,1}}$) points (n being the number of ports), while the one built on the scattering parameters S_{ij} is made of $n(n+1)/2$ complex numbers, with a double RAM/ROM occupation. In addition, the most important point is that any generalized scattering matrix referring to propagating and evanescent modes must satisfy the following conditions for a

lossless network [13]:

$$CP_{i,j} = -CP^*_{j,i} \quad \mathrm{Re}[CP_{i,i}] = 0 \tag{15}$$

where $CP = (I + S)^T J(I - S^*)$ and J is a diagonal matrix with $J_{i,i} = 1$ or j if index i refers to the propagating or evanescent mode, respectively. Hence, an approximated $S_{a\to w}$ matrix, obtained directly by applying the interpolation (12)–(14) to the scattering coefficients, will be affected by some reconstruction errors on its elements and the condition (15) will not be properly satisfied, giving some numerical instabilities.

On the contrary, the $S_{a\to w}$ matrix obtained from the application of the expansion (12)–(14) to the elements of the equivalent circuit properly satisfies (15). In fact, the approximation errors affect only the susceptances b^n_{ij} and the electrical lengths θ_k and not the $S_{a\to w}$ matrix obtained from these values, because $S_{a\to w}$ is the exact scattering matrix relative to the real circuit with given values of b^n_{ij} and θ_k (even if these values could have some reconstruction errors), as discussed in Appendix B for a 2-port circuit.

Having discussed the proposed approach, a database of b^n_{ij} and θ_k, based on $(\frac{d_p}{a}, \frac{w_q}{a}, \frac{f_m}{f_{c,1}})$ points, has been built for the 42-port (21 input and 21 output ports) equivalent circuit of the regular-to-reduced-width waveguide transition and the linear interpolation (12)–(14) for b^n_{ij} and θ_k has been defined. The $S_{a\to w}$ matrix can be evaluated for any point $(\frac{\bar{d}}{a}, \frac{\bar{w}}{a}, \frac{\bar{f}}{f_{c,1}})$ by using (1)–(11).

The knowledge of θ_k, $k = 1, \ldots, 42$ allows us to set the maximum thickness t of the iris that can be analyzed with the 42-port equivalent circuit. In fact, referring to Fig. 1, we can draw the 42-port equivalent circuit of the regular-to-reduced-width waveguide transition placed at $z = 0$ in Fig. 2(a), with a 42-side polygon (the "core") and 42 electrical lines, connecting the "core" of the circuit to the input/output ports. The k-th output port, characterized by the series reactance $-jX_{0k}$ and the electrical line of length $\theta_k = \theta^{out}_k$, is connected to an electrical line of length $a_k t$, corresponding to the k-th evanescent mode of the reduced waveguide of length t and width w placed between $z = 0$ and $z = t$ in Fig. 2(a), with the attenuation constant a_k. Finally, this electrical line "cascade" is connected to the k-th input port of the equivalent circuit of the reduced-to-regular-width waveguide transition, characterized by the series reactance $-jX_{0k}$ and the electrical line length $\theta_k = \theta^{in}_k$, placed at $z = t$ in Fig. 2(a).

Hence, the electrical "distance" between the series reactance $-jX_{0k}$ of the k-th output port of the regular-to-reduced-width waveguide transition, placed at $z = 0$, and the series reactance $-jX_{0k}$

of the k-th input port of the reduced-to-regular-width waveguide transition, placed at $z = t$, is equal to

$$\theta_{tot,k} = \theta_k^{out} + a_k t + \theta_k^{in} \tag{16}$$

Any load Z_L connected to the end of the line of length $\theta_{tot,k}$ is "seen" at the input with an input impedance equal to [9]

$$Z_{in}(\theta_{tot,k}) = jX_{0k} \frac{Z_L + jX_{0k} \tanh(\theta_{tot,k})}{jX_{0k} + Z_L \tanh(\theta_{tot,k})} \tag{17}$$

With $\tanh(\theta_{tot,k})|_{\theta_{tot,k}=10} = 0.9999999959$, we can state from (17) that $Z_{in}(\theta_{tot,k})|_{\theta_{tot,k}=10} = jX_{0k}$ for any connected load Z_L. Hence, $Z_{in}(\theta_{tot,k})|_{\theta_{tot,k}=10}$ resonates with the series reactance $-jX_{0k}$, placed at the input of the line of electrical length $\theta_{tot,k}$, giving a short circuit that deletes the presence of the k-th evanescent port, as discussed in the previous section. Therefore, we can say that $\theta_{tot,k} \geq 10\,\mathrm{Np}$ is the value that permits the effects of the k-th evanescent mode in the discontinuities cascade to be neglected. This value can be used to establish the corresponding minimum thickness t ($t_{\min}$) of the iris that permits the k-th mode to be neglected. Obviously, this minimum value is related to the real combination of ($\frac{\bar{d}}{a}$, $\frac{\bar{w}}{a}$, $\frac{\bar{f}}{f_{c,1}}$), but we can establish the "worst" case in the ranges of variation of ($\frac{d_p}{a}$, $\frac{w_q}{a}$, $\frac{f_m}{f_{c,1}}$), regardless of their real values, as shown in Fig. 3. The dots in Fig. 3 represent the "worst" (minimum) case of the value of $\frac{t}{a}$ that permits the corresponding mode to be neglected: for example, the 3-rd mode can certainly be neglected if $\frac{t}{a} \geq 0.445$, regardless of the real value of the points ($\frac{\bar{d}}{a}$, $\frac{\bar{w}}{a}$, $\frac{\bar{f}}{f_{c,1}}$). The dots seem to lie on two different curves, one relative to the odd order modes and the other to the even ones. This is due to the fact that the odd order modes (TE_{30}, TE_{50}, ...) are more easily excited by the discontinuity than the even order ones (TE_{20}, TE_{40}, ...). For example, if the iris is centered, even order modes are not excited. This lower excitation yields the lower values of $\frac{t}{a}$ which are needed in order to neglect the k-th even mode.

If greater detail is needed, the contour plot of the minimum value of $\frac{t}{a}$, with $\frac{d}{a}$ and $\frac{w}{a}$ as variables and with $\frac{f}{f_{c,1}}$ being fixed at the "worst" case, must be evaluated for every mode. For example, the contour plot relative to the 3-rd mode is shown in Fig. 4. With the help of this plot, the minimum thickness $\frac{t}{a}$ can be established with greater accuracy: for example, with $\frac{d}{a} = 0.4$ and $\frac{w}{a} = 0.4$ we can neglect the 3-rd mode if $\frac{t}{a} \geq 0.21$. Obviously, in this way we obtain a more accurate value of the minimum thickness to be able to neglect the 3-rd mode compared

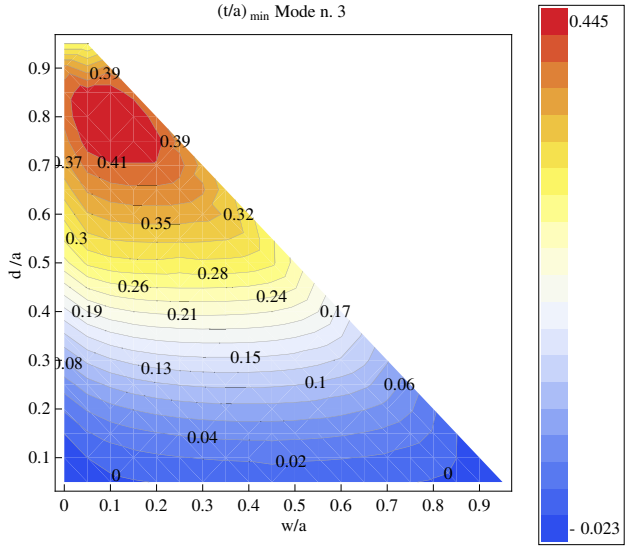

Figure 4. Contour plot of minimum value of $\frac{t}{a}$ to neglect the output evanescent mode n. 3 of the regular-to-reduced-width waveguide transition, placed at $z = 0$ in Fig. 2(a), with $\frac{f}{f_{c,1}}$ being fixed at the "worst" case.

with the value derived from Fig. 3, which can be considered as the limit case to be used without performing any analysis on the real value of $(\frac{d}{a}, \frac{w}{a})$.

It should be noted that the triangular shape of the contour plot is due to the fact that d and w must satisfy $d + w \leq a$. Moreover, the negative values for $\frac{t_{\min}}{a}$ are simply due to the fact that we have set $\theta_{tot,k} = 10\,\text{Np}$ as the condition to evaluate the minimum length $\frac{t_{\min}}{a}$. The areas where $\frac{t_{\min}}{a} < 0$ in Fig. 4 are characterized by $\theta_k^{out} + \theta_k^{in} \geq 10\,\text{Np}$. Hence, the electrical lengths θ_k^{out}, θ_k^{in} are sufficient to satisfy the latter condition, for any value of $\frac{t_{\min}}{a}$.

To confirm the evaluation of the minimum length $\frac{t_{\min}}{a}$, the reflection coefficient amplitude S_{11} of the first iris in Fig. 2(b) is shown in Fig. 5(a) by varying the number of modes chosen in the reduced waveguide of length t, with $a = 22.86\,\text{mm}$, $\frac{d}{a} = 0.25$, $\frac{w}{a} = 0.35$, $\frac{t}{a} = 0.1$. In fact, from Fig. 4 the minimum value for $\frac{t}{a}$ to be able to neglect the third mode is equal to 0.1, for the "worst" value in the range $1.25 \leq \frac{f}{f_{c,1}} \leq 1.9$. This is confirmed in Fig. 5(a) where $|S_{11}|$ is evaluated with 1, 2, 3 or 4 modes in the reduced waveguide, showing that $|S_{11}|$

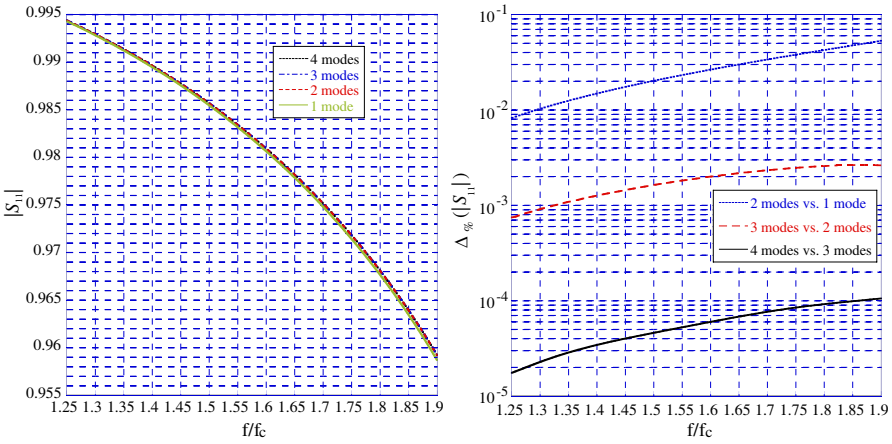

Figure 5. (a) $|S_{11}|$ of a non-centered iris with $a = 22.86\,\text{mm}$, $\frac{d}{a} = 0.25$, $\frac{w}{a} = 0.35$, $\frac{t}{a} = 0.1$, by varying the number of modes in the reduced waveguide of width $\frac{w}{a}$ and thickness $\frac{t}{a}$. (b) Percentage difference (19) between S_{11} evaluated with k modes and k-1 modes.

converges with four modes only. This is highlighted in Fig. 5(b) where the percentage difference between S_{11} evaluated with k modes and k-1 modes is shown

$$\Delta_{\%}(|S_{11}|) = \left| \frac{S_{11}^{k\,\text{modes}} - S_{11}^{k\text{-}1\,\text{modes}}}{S_{11}^{k\,\text{modes}}} \right| * 100 \tag{18}$$

indicating very low differences between the results with 3 modes and 4 modes.

If the "worst" case in the ranges of variation of ($\frac{d}{a}$, $\frac{w}{a}$, $\frac{f}{f_{c,1}}$) were chosen from Fig. 3, the number of modes would be 7, giving a higher value than the one previously obtained. This is obvious because the values reported in Fig. 3 do not take into account the real values of $\frac{d}{a}$, $\frac{w}{a}$ but they refer to all the possible combinations of ($\frac{d}{a}$, $\frac{w}{a}$, $\frac{f}{f_{c,1}}$), giving an overestimation on the number of modes to be used in the evaluation of the scattering parameters. However, Fig. 3 can be adopted when the user prefers to evaluate the S matrix regardless of the real values ($\frac{d_p}{a}$, $\frac{w_q}{a}$, $\frac{f_m}{f_{c,1}}$), without an analysis of the details reported in all the figures similar to Fig. 4 referring to all the modes. In fact, a detailed analysis would require as many contour plots as Fig. 4 as the number of the evanescent accessible modes.

The same approach, based on the built database of b_{ij}^n and θ_k, has been used to simulate the iris cascade shown in Fig. 2(b), setting [4] $d_1 = d_4 = 0$, $w_1 = w_4 = 10.86\,\text{mm}$, $d_2 = 8.5\,\text{mm}$, $w_2 = 6.14\,\text{mm}$, $d_3 = 2\,\text{mm}$, $w_3 = 6.79\,\text{mm}$, $t_i = 2\,\text{mm}$, $i = 1, 2, 3, 4$, $L_1 = 13.74\,\text{mm}$, $L_2 = 15.047\,\text{mm}$, $L_3 = 13.756\,\text{mm}$, $a = 19.05\,\text{mm}$, $b = 9.525\,\text{mm}$. From Fig. 3, we can observe that the value $t_i/a = 0.105$ permits 7 modes to be considered in the reduced waveguide, regardless of the real value of $w_i/a, d_i/a$ of the four irises. The scattering matrices of the four irises have been evaluated from (1)–(11) and the previously built database and interpolation (12)–(14). The four scattering matrices, with proper phase shifts corresponding to the lengths L_i, $i = 1, 2, 3$, have been cascaded to obtain the overall S_{11} of the cascade. This has been compared with the results obtained with a commercial software, CST, and the comparison is shown in Fig. 6, showing good agreement. It should be noted that 4 accessible modes in the three cavities of Fig. 2(b) are sufficient to obtain the curves shown in Fig. 6.

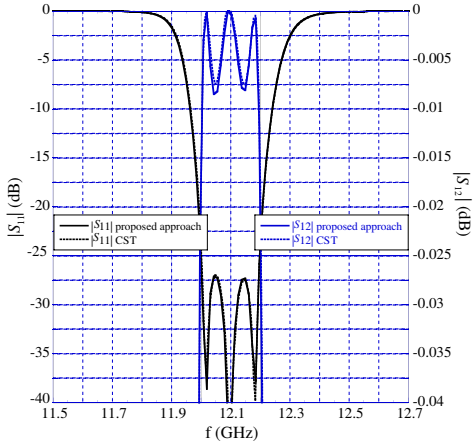

Figure 6. $|S_{11}|$ and $|S_{12}|$ of the four irises cascade shown in Fig. 2(b) obtained with the proposed approach and CST.

The b_{ij}^n and θ_k values of the equivalent circuit have also been obtained for the H-plane bend shown in Fig. 7 with two irises at the input and output section. The whole structure has been divided into the cascade of the input iris, the H-plane bend and the output iris.

The H-plane bend (without irises) has been analyzed with the boundary contour mode-matching method [14, 15] and a numerical code has been developed. The results have been obtained with 21 input modes (one propagating mode and 20 evanescent modes) and 21 output modes ($1 + 20$, as the input).

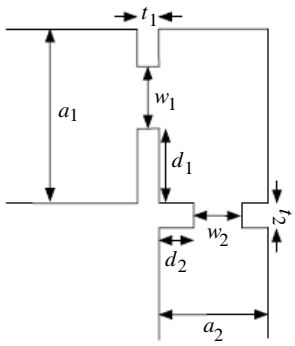

Figure 7. Two irises and an H-plane bend in a rectangular waveguide.

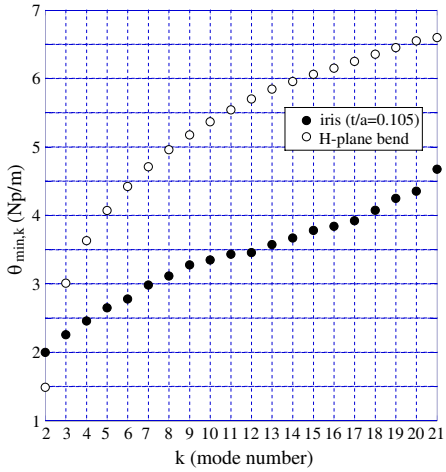

Figure 8. Minimum value of θ_k, $k = 2, 3, \ldots, 21$ ($\theta_{\min,k}$) for the first 20 evanescent modes of (a) H-plane bend and (b) iris with $\frac{t}{a} = 0.105$.

As the irises are directly connected to the H-plane bend, the condition on (16), which has been used to evaluate the minimum length $\frac{t}{a}$ to neglect the k-th mode in the iris, must be replaced by

$$\theta^{out}_{k,iris} + \theta^{in}_{k,bend} \geq 10 \text{ Np} \tag{19}$$

in order to understand how many modes we need to consider in the "cascade" of the iris and the bend. $\theta^{out}_{k,iris}$ and $\theta^{in}_{k,bend}$ are the electrical lengths relative to the k-th evanescent output port of the first iris equivalent circuit and to the k-th evanescent input port of the H-plane equivalent circuit. The minimum value of $\theta^{in}_{k,bend}$ for the H-plane bend in the frequency range $1.25 \leq \frac{f}{f_{c,1}} \leq 1.9$ has been obtained from the

database and it is shown in Fig. 8 with white dots. Moreover, $\theta_{k,iris}^{out}$ has been evaluated for any combination of points $(\frac{d_p}{a}, \frac{w_q}{a}, \frac{f_m}{f_{c,1}})$ in the built database, yielding to the "worst" case shown in Fig. 8 with black dots, for a ratio $\frac{t}{a} = 2/19.05 = 0.105$. Summing the "worst" cases for $\theta_{k,\min}$ relative to the H-plane bend and to the irises with $\frac{t}{a} = 0.105$, we can observe that from the 16-th mode the sum of $\theta_{k,\min}$ of the bend and of the iris is greater than 10 Np. Hence, the overall electrical length of the cascade of the equivalent circuits of the input (or output) iris and the bend can be assumed greater than 10 Np, that has been taken as the limit value to be able to neglect the modes starting from the 16-th one. Hence, the cascade of two irises and the H-plane bend has been analyzed with 16 modes and the S matrices of the two irises and the bend have been evaluated from (1)–(11) and the previously built database and interpolation (12)–(14).

The reflection coefficient amplitude obtained with the proposed approach and with commercial CST software is reported in Fig. 9(a) for $d_1/a = 0.1$, $w_1/a = 0.7$, $d_2/a = 0.3$, $w_2/a = 0.65$, $\frac{t}{a} = 0.105$, $a = 19.05$ mm, $b = 9.525$ mm, showing very good agreement. The

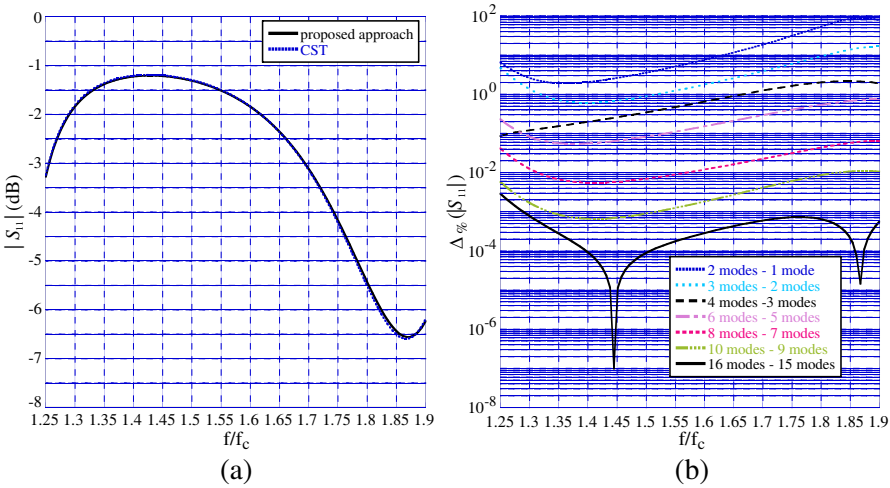

Figure 9. (a) $|S_{11}|$ of two non-centered irises and the H-plane bend, shown in Fig. 7, with $a = a_1 = a_2 = 19.05$ mm, $d_1/a = 0.1$, $w_1/a = 0.7$, $d_2/a = 0.3$, $w_2/a = 0.65$, $\frac{t}{a} = 0.105$ [4] evaluated with the proposed approach based on the equivalent circuits of the two irises and the H-plane bend (continuous line) and commercial CST software (dotted lines). (b) Percentage difference (19) between S_{11} evaluated with k modes and k-1 modes.

convergence of the reflection coefficient is discussed in Fig. 9(b) showing the percentage difference $\Delta_{\%}(|S_{11}|)$ (18) between the evaluation with k modes and k-1 modes: the convergence is quite fast and with ten modes $\Delta_{\%}(|S_{11}|) < 10^{-2}$, which is a very low value that would permit modes from 10 upwards to be neglected. In fact, the 10-th mode has the minimum value of θ_{10} equal to about 9 Np, as can be obtained by summing the "worst" cases in Fig. 8 corresponding to $k = 10$. However, having assumed the limit value equal to 10 Np, we can observe that the 16-th mode has a very good convergence over the whole frequency band, confirming the aforementioned considerations.

Another example of an application of the proposed equivalent circuit is the filter shown in Fig. 10 [4]. The S matrices of the irises and the bends have been evaluated from the built databases with the approach previously discussed, with 16 modes for the bends and the outer part of the irises, and 12 modes for the inner part of the irises (the window of width w). The S matrices have then been cascaded to obtain the overall S matrix of the filter. The amplitude of the scattering parameters seen at the input port are shown in Fig. 11 together with the ones obtained with CST: the curves show good agreement.

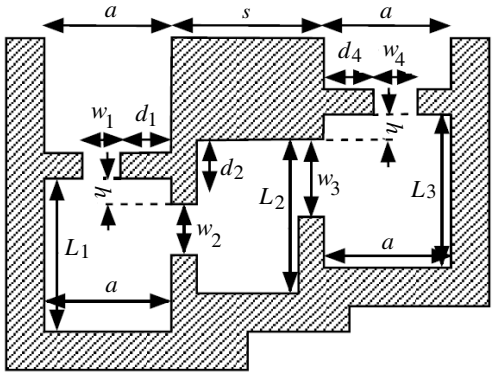

Figure 10. A filter with (all dimensions are in mm): $a = 19.05$, $s = 17.245$, $w_1 = 8.36$, $d_1 = 5.39$, $h = 1$, $L_1 = 14.305$, $w_2 = 5.88$, $d_2 = 6$, $L_2 = 19.05$, $w_3 = 7.19$, $L_3 = 14.13$, $d_4 = 5$, $w_4 = 8.29$ as in Fig. 5 of [4]. The irises are 1 mm thick.

Other structures (the E-plane bend and the capacitive window shown in Figs. 12(a) and 12(b)) have been analyzed with BCMM [14, 15] or the MEN approach [10, 11] (TE_x modes have been considered) and their equivalent circuits have been extracted.

The databases for the E-plane bend for the standard rectangular

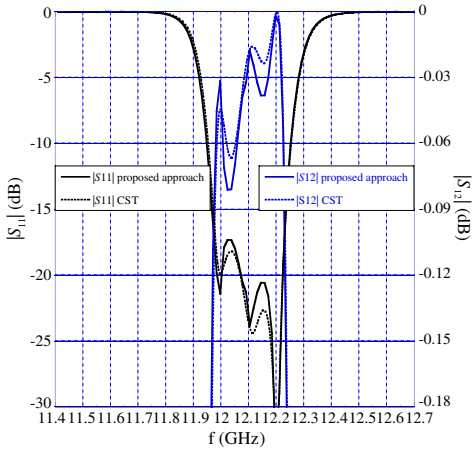

Figure 11. $|S_{11}|$ and $|S_{12}|$ for the filter shown in Fig. 10 (mono-modal range of Fig. 5 in [4]).

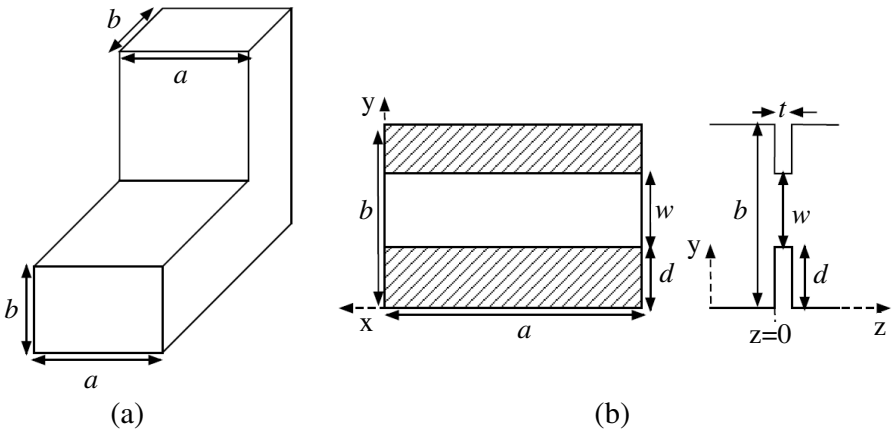

Figure 12. (a) The E-plane bend in rectangular waveguide. (b) The capacitive window in rectangular waveguide.

waveguides have been built and used to evaluate $|S_{11}|$ seen at the input of the E-plane bend, which is shown in Fig. 13 together with that obtained with CST, for the standard rectangular waveguides. The family of rectangular waveguide with $b/a = 0.5$ is emphasized in the caption figure. The CPU time required to build the database was about 220 sec on iMac OSX 10.5 2.66 GHz Intel Core Duo for each standard waveguide (101 points in the frequency range $1.25 < \frac{f}{f_{c,1}} < 1.9$).

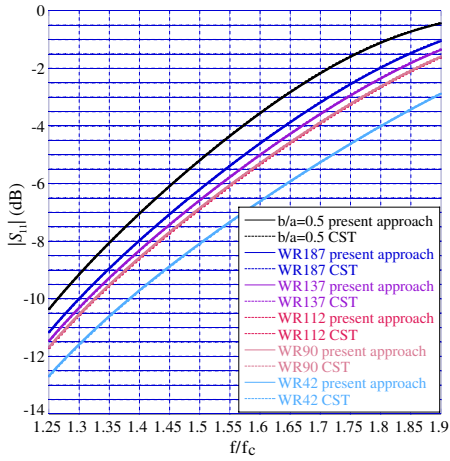

Figure 13. $|S_{11}|$ for the E-plane bend shown in Fig. 12(a). Curve labeled with b/a=0.5 refers to standard waveguides WR229, WR159, WR75, WR62, WR51, WR34, WR28, WR22, WR19, WR15, WR12, WR10, WR8, WR6, WR5, WR4, WR3, being these guides characterized by $b/a = 0.5$.

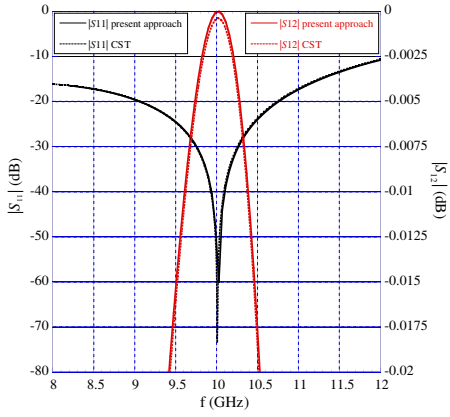

Figure 14. $|S_{11}|$ and $|S_{12}|$ for the cascade of two equal capacitive window in a WR90 waveguide, shown in Fig. 12(b), with $d = 2.1\,\text{mm}$, $w = 5.96\,\text{mm}$, $t = 1\,\text{mm}$, separated by a length $L = 7.9\,\text{mm}$.

The capacitive window shown in Fig. 12(b) has been analyzed with the same approach of the inductive window shown in Figs. 2(a) and 2(b) and its database has been built. A filter characterized by the cascade of two capacitive equal windows with $d = 2.1\,\text{mm}$, $w = 5.96\,\text{mm}$, $t = 1\,\text{mm}$ in a WR90 waveguide, separated by a

length $L = 7.9\,\text{mm}$, has been simulated from (1)–(11) and the built capacitive-window database and with the interpolation (12)–(14). The amplitude of the scattering parameters seen at the input port are shown in Fig. 14 together with the ones obtained with CST: the curves show good agreement. The CPU time required to build the database was about 20 hours on iMac OSX 10.5 2.66 GHz Intel Core Duo for each standard waveguide (50 points in w, 50 points in d (see Fig. 12(b)) and 101 points in the frequency rage $1.25 < \frac{f}{f_{c,1}} < 1.9$). The CPU time to evaluate the scattering parameters for the filter discussed in Fig. 14 was few seconds.

The built databases can be freely used and downloaded at http://leibniz.dii.univpm.it/zappelli/ec/index.html.

4. CONCLUSIONS

The equivalent circuit proposed in [7] has been applied to many complex structures and the expressions of the S matrix for the general n-port circuit have been derived, obtaining very simple formulas which are easily implementable in a source code. Some databases for irises and bends have been evaluated and used to determine the real S matrices of the structures analyzed in the examples, obtaining good agreement with the numerical results evaluated using commercial software, as experimental results are not available.

APPENDIX A.

If the discontinuity output section is characterized by evanescent modes alone, the scattering matrix of the n-port circuit is obtained in terms of the three-port circuit shown in Fig. A1, by matching n-2 evanescent modes at a time, leaving "active" only port 1 (relative to the input propagating mode) and ports k and $i\,(i > k)$ relative to two evanescent accessible modes, which become ports 2 (k) and 3 (i) of the equivalent circuit shown in Fig. A1. Hence, the reduced three-port circuit is described by the following expressions for the scattering parameters

$$S_{11} = -e^{-2j\theta_1} \tag{A1}$$

$$S_{1k} = 2e^{j\pi/4}e^{-j\theta_1-\theta_k} \tag{A2}$$

$$S_{1i} = 2e^{j\pi/4}e^{-j\theta_1-\theta_i} \tag{A3}$$

$$S_{kk} = \left(1 - 2j + 2\sum_{m=i+1}^{n} b_{2m}^{n} + 2\sum_{m=2}^{k} b_{1m}^{n} + 2\sum_{m=3}^{k+1} b_{2m}^{n}\right) e^{-2\theta_k} \tag{A4}$$

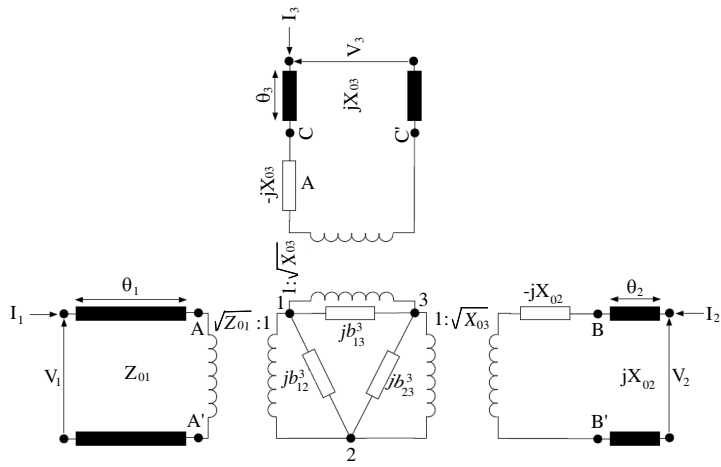

Figure A1. The equivalent three-port circuit for a discontinuity with one input propagating mode (port 1) and two output evanescent modes (ports 2, 3).

$$S_{ki}=2\left(\sum_{m=i+1}^{n} b_{2m}^{n}+\sum_{m=2}^{k} b_{1m}^{n}-j\right)e^{-\theta_k-\theta_i} \tag{A5}$$

$$S_{ii}=\left[1-2j+2\sum_{m=i+1}^{n} b_{2m}^{n}+2\sum_{m=2}^{k} b_{1m}^{n}+2\sum_{l=k+1}^{i}\left(b_{1l}^{n}+\sum_{m=i+1}^{n} b_{lm}^{n}\right)\right]e^{-2\theta_i} \tag{A6}$$

APPENDIX B.

Let us discuss the linear interpolation of the S-parameters relative to a simple circuit, like the one shown in Fig. B1, referring to propagating modes only, which refers to a resonant circuit at $\omega = 1$, with $L = 1$ and $C = 1$ (L and C being normalized quantities with respect to Z_{01} and Z_{02}). The expression for the shunt susceptance, b_p, is easy to obtain. Let us suppose that $\theta_1 = \theta_2 = 0$ in Fig. B1, for simplicity. The exact scattering coefficients are

$$S_{11} = S_{22} = \frac{1-\omega^2}{(\omega-j)^2}\ ,\ S_{12} = S_{21} = -\frac{2j\omega}{(\omega-j)^2} \tag{B1}$$

A linear interpolation (for simplicity) applied to the exact scattering coefficients (B1) in the range $0.5 \leq \omega \leq 1.5$ yields

$$S_{11}^{app} = -0.36 + j0.48 + (0.212 - j0.835)(\omega - 0.5) \tag{B2}$$

$$S_{12}^{app} = 0.64 + j0.48 + (0.212 - j0.835)(\omega - 0.5) \tag{B3}$$

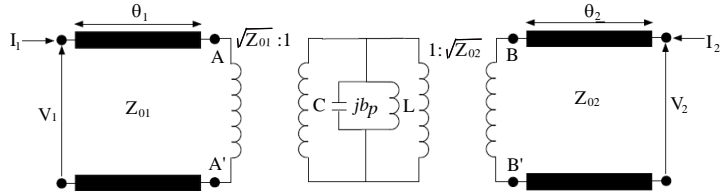

Figure B1. The equivalent two-port circuit for a discontinuity with one input and one output propagating mode.

The approximated scattering parameters are quite different from the exact ones, as could be seen by plotting them, and the effect of the linearization of the scattering coefficients is quite poor. Moreover, the main disadvantage is that the conservation of the real power is not satisfied in the interpolating range. In fact, if we evaluate $|S_{11}^{app}|^2 + |S_{12}^{app}|^2$, which must always be equal to 1 and is equivalent to (15) for propagating modes, we obtain

$$\begin{aligned} &|S_{11}^{app}|^2 + |S_{12}^{app}|^2 \\ &= 2(0.897-0.835\omega)^2+(-0.466+0.212\omega)^2+(0.534+0.212\omega)^2 \neq 1 \end{aligned} \quad \text{(B4)}$$

and this error always affects the interpolated scattering coefficients for any interpolating function chosen (linear, spline, Cauchy, ...).

Let us consider now a different approach to the linearization, as proposed in Section 3. The interpolation is applied to the susceptance b_p in the same range, yielding $b_p^{app}(\omega) = -1.5 + 2.33(-0.5 + \omega)$. The linearized b_p^{app} suffers from reconstruction error as already stated in Section 3, but the effect on the scattering coefficients is different from the previous case. In fact, their expressions, evaluated from (B1), are

$$S_{11}^{b_p} = \frac{2.33(\omega - 0.5) - 1.5}{1.5 + 2j - 2.33(\omega - 0.5)} \quad \text{(B5)}$$

$$S_{12}^{b_p} = \frac{2j}{1.5 + 2j - 2.33(\omega - 0.5)} \quad \text{(B6)}$$

and their real parts, imaginary parts could be plotted, showing that there is a more realistic approximation to the exact values of the scattering coefficients. Moreover, the conservation of the real power, equivalent to (15) for propagating modes, is ensured, as can be obtained from (B5) and (B6):

$$\begin{aligned} &\left|S_{11}^{b_p}\right|^2 + \left|S_{12}^{b_p}\right|^2 \\ &= \frac{[2.33(\omega - 0.5)-1.5]^2}{[2.33(\omega-0.5)-1.5]^2+4} + \frac{4}{[2.33(\omega - 0.5)-1.5]^2 + 4} = 1 \end{aligned} \quad \text{(B7)}$$

Hence, as discussed in Section 3, the linearization on the susceptance has reconstruction errors, but the effect on the scattering coefficients is less destructive than the direct interpolation on the scattering coefficients. Moreover, the conservation of the real power is always satisfied with the proposed approach. Similarly, it can be shown that the S-matrix of a n-port circuit obtained from the application of the expansion (12)–(14) to the elements of the equivalent circuit properly satisfies (15).

REFERENCES

1. Morini, A. and G. Venanzoni, "Scheme for the implementation of cross-couplings for highly tuneable filters," *IEEE Microwave and Wireless Components Letters*, Vol. 22, No. 5, 227–229, 2012.
2. Accatino, L. and M. Mongiardo, "Hybrid circuit-full-wave computer-aided design of a manifold multiplexers without tuning elements," *IEEE Transactions on Microwave Theory and Techniques*, Vol. 50, No. 9, 2044–2047, 2002.
3. Guglielmi, M., "Simple CAD procedure for microwave filters and multiplexers," *IEEE Transactions on Microwave Theory and Techniques*, Vol. 42, No. 7, 1347–1352, 1994.
4. Guglielmi, M., F. Montauti, L. Pellegrini, and P. Arcioni, "Implementing transmission zeros in inductive-window bandpass filters," *IEEE Transactions on Microwave Theory and Techniques*, Vol. 43, No. 8, 1911–1915, 1995.
5. Marcuvitz, N., *Waveguide Handbook*, McGraw-Hill, New York, 1951.
6. Montgomery, C. G., R. H. Dicke, and E. M. Purcell, *Principles of Microwave Circuits*, 1st Edition, McGraw-Hill, 1948.
7. Zappelli, L., "An equivalent circuit for discontinuities exciting evanescent accessible modes," *IEEE Transactions on Microwave Theory and Techniques*, Vol. 60, No. 5, 1197–1209, 2012.
8. Vanin, F. M., D. Schmitt, and R. Levy, "Dimensional synthesis for wide-band waveguide filters and diplexers," *IEEE Transactions on Microwave Theory and Techniques*, Vol. 52, No. 11, 2488–2495, 2004.
9. Collin, R. E., *Field Theory of Guided Waves*, IEEE/OUP Series on Electromagnetic Wave Theory, 1996.
10. Gerini, G. and M. Guglielmi, "Efficient integral equation formulations for admittance or impedance representation of planar waveguide junctions," *IEEE MTT-S International Microwave Symposium Digest*, Vol. 3, 1747–1750, Jun. 1998.

11. Gerini, G. and L. Zappelli, "Phased arrays of rectangular apertures on conformal cylindrical surfaces: A multimode equivalent network approach," *IEEE Transactions on Antennas and Propagation*, Vol. 52, No. 7, 1843–1850, 2004.
12. Collin, R., *Foundations for Microwave Engineering*, McGraw-Hill, 2001.
13. Morini, A. and T. Rozzi, "On the definition of the generalized scattering matrix of a lossless multiport," *IEEE Transactions on Microwave Theory and Techniques*, Vol. 49, No. 1, 160–165, 2001.
14. Reiter, J. M. and F. Arndt, "A boundary contour mode-matching method for the rigorous analysis of cascaded arbitrarily shaped H-plane discontinuities in rectangular waveguides," *IEEE Microwave and Guided Wave Letters*, Vol. 2, No. 10, 403–405, 1992.
15. Reiter, J. M. and F. Arndt, "Rigorous analysis of arbitrarily shaped H- and E-plane discontinuities in rectangular waveguides by a full-wave boundary contour mode-matching method," *IEEE Transactions on Microwave Theory and Techniques*, Vol. 43, No. 5, 796–801, 1995.